energies

MDPI

Article

Improved Electrical and Structural Stability in HTL-Free Perovskite Solar Cells by Vacuum Curing Treatment

Salvatore Valastro [1,2], Emanuele Smecca [1], Salvatore Sanzaro [1], Filippo Giannazzo [1], Ioannis Deretzis [1], Antonino La Magna [1], Youhei Numata [3], Ajay Kumar Jena [3], Tsutomu Miyasaka [3], Antonio Gagliano [2] and Alessandra Alberti [1,*]

[1] CNR-IMM, 95121 Catania, Italy; salvatore.valastro@imm.cnr.it (S.V.); emanuele.smecca@imm.cnr.it (E.S.); salvatore.sanzaro@imm.cnr.it (S.S.); filippo.giannazzo@imm.cnr.it (F.G.); ioannis.deretzis@imm.cnr.it (I.D.); antonino.lamagna@imm.cnr.it (A.L.M.)

[2] Department of Electrical, Electronic and Computer Engineering, University of Catania, 95125 Catania, Italy; agagliano@dii.unict.it

[3] Graduate School of Engineering, Toin University of Yokohama, Yokohama, Kanagawa 225-8503, Japan; y_numata@toin.ac.jp (Y.N.); jenajay@gmail.com (A.K.J.); miyasaka@toin.ac.jp (T.M.)

* Correspondence: alessandra.alberti@imm.cnr.it

Received: 10 July 2020; Accepted: 30 July 2020; Published: 1 August 2020

Abstract: Device engineering with proper material integration into perovskite solar cells (PSCs) would extend their durability provided a special care is spent to retain interface integrity during use. In this paper, we propose a method to preserve the perovskite (PSK) surface from solvent-mediated modification and damage that can occur during the deposition of a top contact and furtherly during operation. Our scheme used a hole transporting layer-free top-contact made of Carbon (mostly graphite) to the side of hole extraction. We demonstrated that the PSK/graphite interface benefits from applying a vacuum-curing step after contact deposition that allowed mitigating the loss in efficiency of the solar devices, as well as a full recovery of the electrical performances after device storage in dry nitrogen and dark conditions. The device durability compared to reference devices was tested over 90 days. Conductive atomic force microscopy (CAFM) disclosed an improved surface capability to hole exchange under the graphite contact after vacuum curing treatment.

Keywords: photovoltaics; perovskite; durability; X-ray diffraction (XRD); CAFM; I-V (current - voltage) curve; storage; recovery; vacuum treatment; interfaces; stability

1. Introduction

Perovskite solar cells (PSCs) have been representing a scientific and technological breakthrough since their birth in 2009, when Miyasaka et al. used hybrid perovskites in a photon-to-current conversion device for the first time, achieving an efficiency of 3.8% [1,2]. In 10 years, PSCs have reached a maximum efficiency of 25.2% [3], which is indeed approaching the record on silicon solar cells. Recently applied in tandem solar cells with silicon, PSC/silicon tandem solar cells are approaching the single junction Shockley-Queisser limit and even promise to go further. The current record has been raised up to 28% by Oxford Photovoltaics Limited (Oxford PV) [4] and further to 29.1% by Helmholtz-Zentrum Berlin (HZB) [3] in monolithic two-terminal architectures. Furthermore, mechanically stacked two-terminal solar cells, that overcome some critical technological constraints, have reached an efficiency of 26.3% in recent months [5]. Despite these

positive features, the poor stability and limited durability are the main obstacles which must be overcome for the commercialization of PSCs.

Device engineering has a crucial part in the reliability and integrability of the PSC technology and therefore it deserves special consideration. In direct architecture (Transparent conductive oxide (TCO)/electron-transporting layer (ETL)/perovskite/hole-transporting layer (HTL)/counter electrode (CE)), researchers focus particular attention on the choice of the HTL and of the CE, having an important role in the performance stability of the devices. Specifically, the interfacial degradation, occurring at the CE/HTL and the HTL/perovskite interfaces, is the main reason for the decrease in PSC efficiency over time, while degradation of the core of the perovskite layer is expected to have a minor effect [6]. As a matter of fact, most of the efficient and highly expensive organic hole-transporting materials (HTMs) (e.g., Spiro-OMeTAD) are operationally unstable and are inclined to mediate migration of halide and metal ions of noble metal counter-electrodes which are conventionally used (e.g., Au, Ag, and Al) [7–9]. Among the non-conventional proposed architectures, hole-transporting-layer-free Carbon-based PSCs (HTL-free C-PSCs) are promising candidates due to their superior long-term stability and low cost [10–13] that compensate the lack of carrier selectivity with respect to the application of a hole transporting material. Carbon-based top contacts for HTL-free PSCs are made using carbon pastes (mix of graphite flakes, carbon black, curing resin and solvent) deposited directly on the perovskite layer by different methods: doctor-blading, ink-jet printing, hot-press transfer, etc. [14]. These methods are up-scalable and low-cost, thus providing a feasible industrially appealing solution for large area devices. Furthermore, the structural stability and the hydrophobic character of the carbon electrode, preserving the underneath perovskite from the environmental humidity, make it a promising back-contact for commercialization of PSCs. Recently, in order to improve the efficiency of HTL-free devices, various p-type doping approaches have been investigated in C-electrodes to regulate the Fermi-level of the carbon electrode and to make it more selective for holes extraction [11]. A different strategy, ideated by Zhou et al. [15], consists of substituting the state-of-art ETL used in HTL-free carbon based devices, namely TiO_2, with solution processed hexamethonium bromide (HMB)-doped C_{60} reaching a power conversion efficiency (*PCE*) of over 16%, the highest value in literature for this architecture of devices. In 2019, in the context of up-scalable approaches, Barichello et al. [16] designed a fully printable HTL-free C-PSC using a home-made mesopourous alumina (Al_2O_3) ink, achieving a maximum efficiency of 9.13% and reaching 10.66% with a water treatment of substrate before perovskite deposition. However, the optimization of the carbon deposition method for PSCs with a long durability has been rarely explored in the literature.

In order to improve long-term stability of the electrical performance in PSCs, the perovskite interface with the carbon electrode must be preserved from degradation [17–21]. As a matter of fact, PSCs with carbon contacts deposited by the doctor-blading (DB) method and successive annealing show a deterioration path of the electrical performance during time, primarily due to a solvent-mediated interaction of the C-electrode with the perovskite surface [22]. In our previous work [23], we found that the preservation of this interface can be achieved with a solvent-free deposition method based on hot-pressing (HP) a free-standing dried C-Al foil directly on the perovskite layer (HP-PSC). The method resulted in an improved long-term stability of the device efficiency with respect to the one applying DB C-contact. As a drawback, HP transfer methods could pose some long-term practical issues, such as the non-perfect local adhesion of the C-Al contact on the underlying perovskite, especially crucial in large area devices. Hence, new post-deposition treatments are needed for doctor-bladed Carbon contacts in order to prevent the degradation that can occur at the interface with the perovskite.

Herein, we investigate a simple fabrication method for the Carbon contact consisting of doctor-blading deposition ($T_{annealing}$ = 100 °C) and successive vacuum-curing treatment for 24 h (samples are hereafter called DBv-PSCs). The use of vacuum-curing treatment has been recently reported in the literature for PCBM/Cu selective contacts [24]. The positive effect on the stability of devices was there associated with a reduction of amorphous regions in the methylammonium lead iodide ($MAPbI_3$) layer to the benefit of the contact/perovskite interface quality. In our treatment, we apply a mild

underpressure of 10^{-2} mbar for 24 h on the devices, differently from the work of Ref. [24], where a long-lasting vacuum treatment was used (100 h) and high vacuum conditions (10^{-6} mbar) were needed. As a further difference, we do not remove and then re-deposit the contact layer after vacuum curing, therefore proposing a simplified fabrication procedure. The day-by-day performance comparison with a non-vacuum-treated representative device (DB-PSC), along a timescale of 30 days, shows the positive effect of the vacuum curing treatment on the device stability. The investigation was extended up to 90 days after the device fabrication. Additionally, in order to compare the conditions of the perovskite and its surface under the carbon contact of the DBv-PSC to those of the DB-PSC, X-ray diffraction (XRD) and Conductive atomic force microscopy (CAFM) measurements are performed.

Our approach offers a feasible and simple strategy to fabricate the carbon contact by the doctor-blading method avoiding the typical degradation path of DB-made devices caused by the harmful action over time of the solvent present in commercial C-pastes. Thanks to the vacuum-curing treatment, the preservation of the Carbon/perovskite interface and, consequentially, an improvement of performance stability are achieved.

2. Materials and Methods

Figure 1a shows a ~450 nm-thick $MAPbI_3$ layer deposited by solution processing on a ~90 nm-thick meso-porous-TiO_2 (mp-TiO2) on compact-TiO_2 (c-TiO_2)/ fluorine doped tin oxide (FTO). Before preparation of the perovskite film, a perovskite precursor solution and the substrates were warmed at 70 °C. A 1.5 M solution of methylammonium iodide (MAI, 99.0%, Tokyo Chemical Industry, Tokyo, Japan) and lead iodide (PbI_2, 99.99%, trace metals basis, Tokyo Chemical Industry, Tokio, Japan) (1:1 in mol) in N, N-dimethylformamide (DMF) and dimethylsulfoxide (DMSO) (4:1 *v*/*v*) was poured onto the TiO_2 mesoporous substrate and spin-coated (kept for 60 s; 5000 rpm for 30 s with chlorobenzene dripping). The as-prepared film was pot-roast vapor annealing (PR-VA)-treated at 100 °C for 10 min on a hot plate. The resulting perovskite layer was compact and uniform. The size of the grains was in the range of 400–800 nm. Finally, a 30 μm-thick carbon contact (carbon paste DN-CP01 by Dyenamo, Stockholm, Sweden) was deposited on the FTO/c-TiO_2/mp-TiO_2/$MAPbI_3$ multilayer by the doctor-blading technique and successively annealed at 100 °C for 15 min (DB-PSC). For selected vacuum-treated solar cells (DBv-PSC), we applied 10^{-2} mbar for 24 h to the device inside a small vacuum chamber. Both kinds of prepared devices, with and without vacuum-treatment, were taken without encapsulation for the entire experiment. The schematic representation of the preparation process of vacuum-cured perovskite solar cells (DBv-PSCs) is shown in Figure 1b.

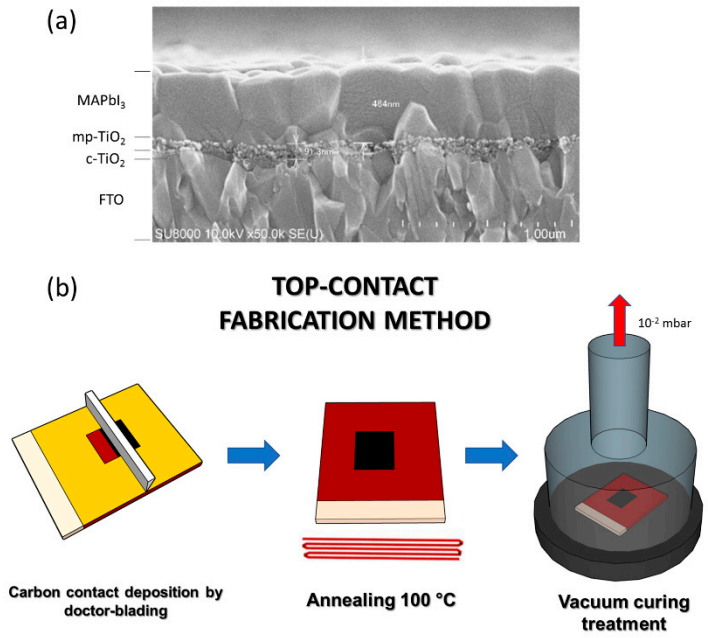

Figure 1. Top-contact fabrication method**:** (**a**) Cross-sectional scanning electron microscopy (SEM) image showing the $MAPbI_3$ layer with large grains and a flat interface with the electron-transporting layer (ETL); (**b**) Schematic of top-contact fabrication on a perovskite solar cell (PSC) and successive vacuum curing treatment.

A systematic investigation of the electrical response of representative vacuum cured devices was done by monitoring the performances for 30 days in comparison with reference no-vacuum-treated devices. Measurements were made once per day, acquiring current density-voltage (J-V) characteristics under simulated sunlight.

Table 1 illustrates the operative parameters for solar cell characterization, the aging conditions and the measurements made in order to follow the evolution of device performances during time. The aging conditions are based on International Summit on Organic Photovoltaic Stability-dark storage studies-level 1 (ISOS-D-1) protocol [25], with the only difference that our cells, after the measurement in air, were kept in nitrogen instead of ambient conditions. That was a precise choice to highlight exclusively the role of the Carbon/perovskite interface without additional effects due toexposure to humidity. The storage in nitrogen environment, in fact, preserves the $MAPbI_3$ from degradation during storage [17]. X-ray diffraction analyses were performed after recursive peeling of the carbon contact up to complete removal by an adhesive tape (3M, Saint Paul, Minnesota, USA) in order to explore the entire layer structure and the eventual effect of the vacuum curing treatment. Atomic force microscopy (AFM) was also used to investigate the perovskite surface morphology after carbon contact removal in comparison to the one outside the contact area. Current maps were acquired by conductive atomic force microscopy (CAFM) using a Platinum (Pt) tip to extract a current of holes from the perovskite layer inside and outside the contact regions.

Table 1. Parameters used for solar cell characterization, frequency of analyses and aging conditions (similar to International Summit on Organic Photovoltaic Stability-dark storage studies-level 1 (ISOS-D-1) protocol).

Solar cell characterization	Type of measurements	J-V curves
	Light source type	Simulated sunlight (Peccell PEC-L01)
	Intensity	100 mW/cm^2
	Spectrum	AM 1.5
	Filters applied	No
	Active area	0.25 cm^2 (mask)
	Range measurements	from −0.1 V to 1.2 V
	ΔV	0.01 V
	Scan speed	0.50 mV/s
	Atmosphere of measurements	Air
	Humidity	55%
	Temperature	24 °C
	Direction	Forward and reverse
	Preconditioning	No
Aging conditions	Light	No
	Temperature	24 °C
	Atmosphere	N_2
	Electrical bias condition	No bias
	Encapsulation	No
	Comply with known protocols	Similar to ISOS-D1 (but aging in N_2 not in air)
Measurements during ageing	Type of measurements	J-V curves
	Recording frequency	Once per day for one month

3. Results and Discussion

Figure 2a shows the initial performance (day 1) of a representative DBv-PSC compared to a reference device, namely a DB-PSC which was not treated in vacuum after C-deposition. We notice that both devices start working with similar initial power conversion efficiency (*PCE*). The DBv-PSC exhibits an efficiency of 6.95% (6.94% for the DB-PSC) with short-circuit photocurrent density (J_{sc}) = 14.42 mA/cm^2 (15.65 mA/cm^2 for the DB-PSC), open-circuit voltage (V_{oc}) = 0.99 V (0.96 V for the DB-PSC), and fill factor (*FF*) = 48.7% (46.2% for the DB-PSC), as shown in Table 2. Such close similarity of the PV parameters, that fall well within the statistics of the single kind of device, indicates that the vacuum treatment does not have any negative effect on the photovoltaic performances.

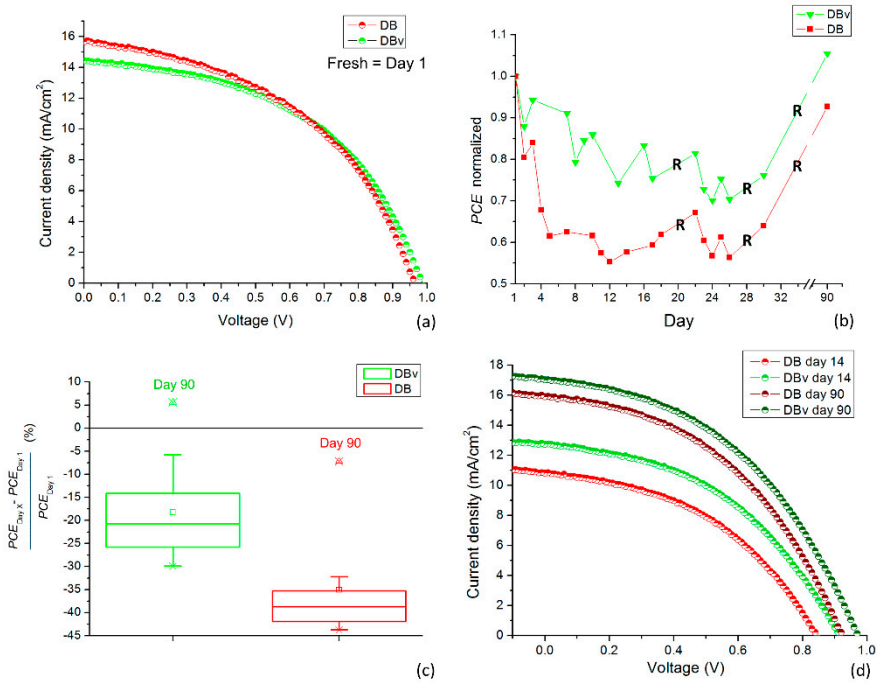

Figure 2. Performances over time in DB-PSC and DBv-PSC: (**a**) Current density-voltage (J-V) curves of representative doctor-blading (DB)-PSC and DBv-PSC at day 1, i.e., with fresh devices; (**b**) *PCE* trend along 30 days and after 60 days storage in dark condition and nitrogen environment. "R" in the figure indicates the partial recovery of performance due to dark storage in nitrogen environment for a time ≥4 days; (**c**) Box plot of *PCE* Percent variations with respect to the value of day 1; (**d**) J-V curves of representative DB-PSC and DBv-PSC (as in Figure 2a) at day 14 and day 90. Measurements were taken on the same device for each type (DB-PSC and DBv-PSC).

Table 2. Photovoltaic parameters of representative DB-PSC and DBv-PSC on day 1 (fresh), day 14 (worst condition), and day 90 taken on the same device for each type (DB-PSC and DBv-PSC).

		Voc (V)	*Jsc* (mA/cm²)	*FF* (%)	*PCE* (%)
Day 1	DB-PSC	0.96	15.65	46.2	6.94
	DBv-PSC	0.99	14.42	48.7	6.95
Day 14	DB-PSC	0.85	10.83	43.52	4.01
	DBv-PSC	0.92	12.73	44.02	5.16
Day 90	DB-PSC	0.92	15.93	44.00	6.45
	DBv-PSC	0.97	17.05	44.38	7.34

The temporal trend of the *PCE* normalized to the value on day 1 is shown in Figure 2b. Relative increase or decrease of the *PCE* of each device is ascribable to degradation/recovery paths. Here, relative recovery of performances occurring in a time interval ≥4 days of storage in dark and nitrogen environment is marked as "R".

In general, in the DB-PSC, a short-lasting performance degradation transient was observed, with a 40% *PCE* loss with respect to the initial value within ~5 days. From day 5 to day 30, the device shows deterioration/recovery behavior and the *PCE* accordingly fluctuates in the range 55–65% of the value on day 1. On the other hand, vacuum curing impacts the long-term stability of the PSC positively, resulting in better efficiency stability over time compared to DB-PSC. In the end, the vacuum-cured PSC indeed loses in average ~20% of the initial *PCE* value, as also shown in the box plots in Figure 2c. This is similar to what we have observed in PSCs with a carbon electrode made by solvent-free hot-press transfer method (HP-PSC) [23]. Moreover, contrary to the DB-PSC, the DBv-PSC does not show the degradation transient behavior in the first days. Since day 1, it exhibits the degradation/recovery pathways similarly to what happens for HP-PSC [23].

On day 30, both kinds of devices were stored in dark conditions, with no bias applied and in a nitrogen environment. After 60 days of storage, both DB-PSC and DBv-PSC were measured to evaluate their "aged" performances. It is noteworthy that both cells have instead recovered their performances in comparison with the last run of measurements. A similar effect is reported in our previous work wherein the top contacts were made without HTL, with the maximum gain achieved by avoiding solvent-perovskite interaction during contact fabrication [23]. In this regard, doctor-blading compared to the hot-press transfer method provides a better guarantee of adhesion to the underlying perovskite through the whole contact area and it is thus believed to be technologically more reliable.

Furthermore, as shown in Figure 2b, the performances of the DBv-PSC on day 90 are even better than those on day 1, with an increase of the *PCE* value by ~6% (7.34% vs. 6.95%), as opposite to what happens to the DB-PSC (decrease of *PCE* values by ~6%). Figure 2c shows the distributions of percent variations of *PCE* from day 1 up to day 90, displayed as box-plots, with respect to the value on day 1 for the DB-PSC and the DBv-PSC. The average values, represented by the horizontal lines in the figure, are −20% and −40% for the DBv-PSC and the DB-PSC, respectively, indicating a minor loss of performances for vacuum-treated devices. The values recorded in the DBv-PSC are more widely scattered than those of the DB-PSC, resulting in a larger box. This is due to better efficiency recovery in the DBv-PSC case. Finally, the outliers in Figure 2c present the *PCE* percent variations after 60 days of storage/measured on day 90. The DBv-PSC shows a surprising *PCE* increase by ~6% (value higher than the zero line) as opposite to the DB-PSC (about −6%).

Figure 2d compares the J-V curves of the two kinds of devices on day 14 (worst condition) and day 90 (final condition). Table 2 summarizes the values of photovoltaic parameters (open circuit voltage, short current density, fill factor and *PCE*) for both DB-PSC and DBv-PSC on day 1, day 14, and day 90. A huge improvement of all photovoltaic parameters is observed on day 90 (after 60 days of storage in dark conditions with no bias applied and in nitrogen environment) compared to values on day 14.The increase in *Jsc* of the vacuum-treated device is especially noteworthy (Figure 2a).

The observed electrical phenomenon likely arises from improved perovskite lattice structure that could also involve the interface with the contacting material. However, the extra-gain introduced by the vacuum treatment indicates that the self-healing of the perovskite core [26], which would occur in both kinds of device, is not an exhaustive explanation. To understand the origin, the Carbon contacts were removed by a process of progressive peeling using a sticky tape (Figure 3a) on day 90 after the last J-V measurements. The structural, morphological and electrical changes of the exposed $MAPbI_3$ surface were analyzed. The composition inside the contact regions was unfolded by X-ray diffraction, as shown in Figure 3b**.** The measurements reveal the same amount of $MAPbI_3$ (main peak at $2\theta = 14.1°$) and almost negligible traces of PbI_2 (main peak at $2\theta = 12.7°$) in both kinds of devices, suggesting no irreversible macroscopic degradation in the perovskite layer under the carbon contact. Our finding indeed moves the focus towards the carbon/perovskite interface. This interface could be pivotal in improving the stabilty of the device, in agreement with the recent literature on other cell architectures [6,27,28].

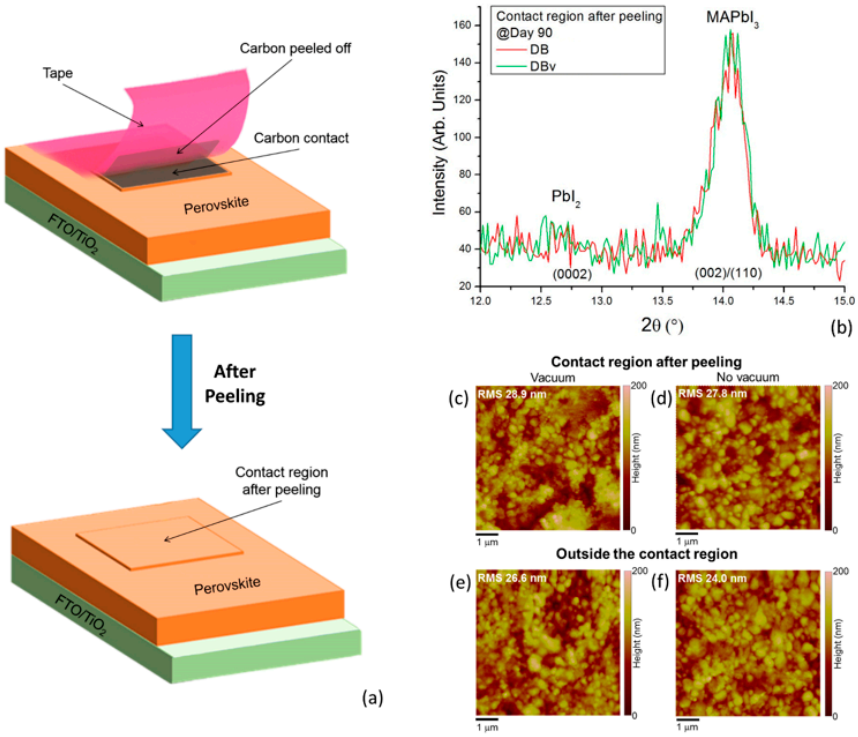

Figure 3. Bulk and surface analyses of the perovskite layer after carbon contact removal: (**a**) Schematic of the carbon contact removal by peeling; (**b**) XRD patterns of representative DB-PSC and DBv-PSC acquired at day 90 inside the contact region after peelings. The diffraction patterns are labeled with the related Miller indexes of the hexagonal (PbI_2) and tetragonal ($MAPbI_3$) phases. Atomic force microscopy (AFM) morphologies inside (**c**),(**d**) and outside (**e**),(**f**) the contact region after peeling in DB-PSC and DBv-PSC.

We have thus investigated the morphology of the $MAPbI_3$ surface by atomic force microscopy (AFM) measurements in different regions, namely inside and outside the contact area after peeling. The morphological analyses on representative devices show negligible differences between the DBv-PSC and the DB-PSC (Figure 3c–f) in both regions, with no evident changes in grain size and roughness. On this basis, we conclude that no significant morphological changes have occurred after deposition of the carbon contact by the doctor-blading method, during vacuum curing and after the contact peeling.

Surface morphology and electrical behavior are not necessarily correlated. To go deeper into the process of carrier extraction from the perovskite surface, local electrical analyses using conductive atomic force microscopy (CAFM) were performed. CAFM was applied to explore the electrical behavior of the $MAPbI_3$ surface at the nanometre scale both inside and outside the contact region after peeling. Local current mapping of $MAPbI_3$ surfaces, as illustrated in Figure 4a, was collected by CAFM using a Pt-coated Silicon tip**.** By applying a positive bias to the electrode, holes are extracted owing to a proper band position of Pt with respect to $MAPbI_3$. All the measurements have been performed under dark conditions.

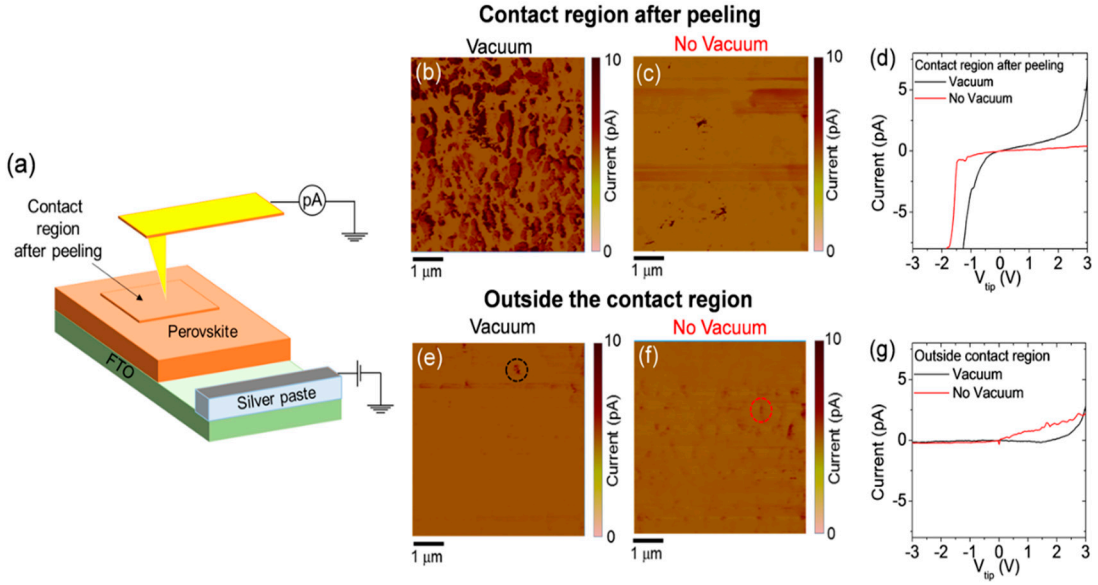

Figure 4. Conductive atomic force microscopy (CAFM) measurements: (**a**) Schematic of conductive atomic force microscopy (CAFM) measurements; Current maps (**b**), (**c**) and local intensity current-voltage (I-V) measurements (**d**) in the region of the contact after peeling for DBv-PSCand for DB-PSC. Current maps (**e**), (**f**) and local I-V measurements, in the areas indicated by black (DBv-PSC) and red (DB-PSC) circles, outside the contact region (**g**).The maps are taken at a fixed voltage of 3 V.

From the CAFM maps, it is clear that higher currents flow-out through the Pt-tip in the contact region of the DBv-PSC (Figure 4b) while the DB-PSC (Figure 4c) counterpart shows low current flow. The more efficient hole extraction from the perovskite surface inside the contact region (after C-contact peeling) in vacuum-treated devices is confirmed by the local I-V measurements shown in Figure 4d. From the shape of the electrical curve, we notice that the rectifying behavior of the tip-perovskite interface and the higher collected current at a fixed voltage in the forward scan ($V > 0$), compared to the reference DB-PSC. Both devices in the area outside the peeled C-contact region exhibit similar electrical response and are less performing than the perovskite surface after peeling in the vacuum-treated devices.

The positive role of the vacuum treatment was indeed clearly stated by the improved quality of the perovskite surface under the C-contact to release holes. We argue this effect to be partially linked to a positive action of the vacuum to further remove residual solvent from the contact after doctor-blading deposition. This is in agreement with the findings of our previous publication, wherein the solvent was prevented to interact with the perovskite layer by applying a hot-press method [23]. Additional positive effects linked to carbon interacting and stabilizing the perovskite surface through modifications at the atomic scale cannot be excluded.

4. Conclusions

We applied a simple method to improve the reliability of doctor bladed C-contacts in HTL-free PSCs. We demonstrated that a mild vacuum treatment after C-deposition has an effect beyond what is solely ascribable to perovskite self-healing occurring within the layer. This effect, instead, mostly relates to the PSK/C-contact interface and impacts on its preservation over time. As a matter of fact, vacuum-cured devices exhibited better long-time stability in comparison to the reference DB-PSCs (without vacuum treatment). The behavior of DBv-PSCs is similar to the one previously observed in PSCs with carbon electrode made by solvent-free hot-press transfer method (HP-PSC). Similarly to the HP-PSC, but contrarily to the DB-PSC, the DBv-PSC does not show the degradation transient behavior in the first days but, since day 1, it has exhibited a degradation/recovery pathway, with recovery being very pronounced. In this respect, doctor-blading, compared to the hot-press transfer method, provides a better guarantee of adhesion to the underlying PSK through the whole contact

area and indeed would be technologically more reliable. A recovery and further improvement of performances after 60 days of storage were observed in the DBv-PSC under nitrogen and in dark without bias. The further improvement observed on day 90 above the starting efficiency value is also noteworthy. Being observed on the same device, this special rise of performances can be trusted. It was mainly ascribed to a rearrangement and stabilization of the PSK/C-contact interface during storage. This was argued by CAFM with local I-V measurements to evaluate the hole extraction from the PSK. Better hole extraction in vacuum-treated PSK surfaces was indeed clearly stated by local I-V curves and current mapping.

Our approach based on a mild vacuum treatment offers a feasible and simple strategy to fabricate the carbon contact by the doctor-blading method and to preserve the Carbon/perovskite interface for a better and longer device reliability.

Author Contributions: Conceptualization, A.A.; methodology, S.V., A.A.; validation, S.V., Y.N. and A.J.; formal analysis, S.V.; investigation, S.V., S.S., E.S., F.G.; resources, A.A. Y.N., A.J.; data curation, S.V.; writing—original draft preparation, S.V. and A.A.; writing—review and editing, A.L.M, I.D., A.G.; supervision, A.A., T.M.; project administration, A.A. and T.M.; funding acquisition, A.A., T.M. and A.L.M. All authors have read and agreed to the published version of the manuscript. All authors have read and agreed to the published version of the manuscript.

Funding: The project was partially supported by the Italian project BEYOND NANO Upgrade (CUP G66J17000350007) and by the bilateral project on PSC (CUP B56C18001070005), co- founded by CNR (Italy) and JSPS (Japan). CNR gratefully acknowledges the project PON entitled "Tecnologia per celle solari bifacciali ad alta Efficienza a 4 terminali per utility scale", called BEST-4U, financed by the Italian Ministry MIUR (CUP B88D19000160005) and the Project PON ARS01_01007 entitled EleGaNTe Electronics on GaN-based Technologies, (CUP B91G18000200005).

Conflicts of Interest: The authors declare no conflict of interest.

References

1. Kojima, A.; Teshima, K.; Shirai, Y.; Miyasaka, T. Organometal Halide Perovskites as Visible-Light Sensitizers for Photovoltaic Cells. *J. Am. Chem. Soc.* **2009**, *131*, 6050–6051.
2. Jena, A.K.; Kulkarni, A.; Miyasaka, T. Halide Perovskite Photovoltaics: Background, Status, and Future Prospects. *Chem. Rev*. **2019**, *119*, 3036–3103.
3. Best Research-Cell Efficiency Chart. Available online: https://www.nrel.gov/pv/cell-efficiency.html (accessed on 3 June 2020).
4. Oxford PV perovskite solar cell achieves 28% efficiency. Available online: https://www.oxfordpv.com/news/oxford-pv-perovskite-solar-cell-achieves-28-efficiency (accessed on 3 June 2020).
5. Lamanna, E.; Matteocci, F.; Calabrò, E.; Serenelli, L.; Salza, E.; Martini, L.; Menchini, F.; Izzi, M.; Agresti, A.; Pescetelli, S.; et al. Mechanically Stacked, Two-Terminal Graphene-Based Perovskite/Silicon Tandem Solar Cell with Efficiency over 26%. *Joule* **2020**, *4*, 1–17.
6. Jena, A.K.; Numata, Y.; Ikegami, M.; Miyasaka, T. Role of spiro-OMeTAD in performance deterioration of perovskite solar cells at high temperature and reuse of the perovskite films to avoid Pb-waste. *J. Mater. Chem. A* **2018**, *6*, 2219–2230.
7. Chen, H.; Yang, S. Carbon-Based Perovskite Solar Cells without Hole Transport Materials: The Front Runner to the Market? *Adv. Mater.*, **2017**, *29*, 1603994.
8. Kim, S.; Bae, S.; Lee, S.; Cho, K.; Lee, K.D.; Kim, H.; Park, S.; Kwon, G.; Ahn, S.; Lee, H.; et al. Relationship between ion migration and interfacial degradation of $CH_3NH_3PbI_3$ perovskite solar cells under thermal conditions. *Sci. Rep.* **2017**, *7*, 1200.
9. Domanski, K.; Correa-Baena, J.P.; Mine, N.; Nazeeruddin, M.K.; Abate, A.; Saliba, M.; Tress, W.; Hagfeldt, A.; Grätzel, M. Not All That Glitters Is Gold: Metal-Migration-Induced Degradation in Perovskite Solar Cells. *ACS Nano* **2016**, *10*, 6306–6314.
10. Cai, Y.; Liang, L.; Gao, P. Promise of commercialization: Carbon materials for low-cost perovskite solar cells. *Chin. Phys. B* **2018**, *27*, 018805.
11. Chen, H.; Yang, S.J. Methods and strategies for achieving high-performance carbon-based perocskite solar cells without hole transport materials. *Mater. Chem. A* **2019**, *7*, 15476–15490.

12. Hadadian, M.; Smått, J.; Correa-Baena, J.P. The role of carbon-based materials in enhancing the stability of perovskite solar cells. *Energy Environ. Sci.* **2020**, *13*, 1377–1407.
13. Babu, V.; Fuentes P.R.; Ahmad, T.; Alvarez, A.O.; Castriotta, L.A.; di Carlo, A.; Fabregat-Santiago, F.; Wojciechowski, K. Improved Stability of Inverted and Flexible Perovskite Solar Cells with Carbon Electrode. *ACS Appl. Energy Mater.* **2020**, *3*, 5126−5134.
14. Fagiolari, L.; Bella, F. Carbon-based materials for stable, cheaper and large-scale processable perovskite solar cells. *Energy Environ. Sci.* **2019**, *12*, 3437–3472.
15. Zhou, J.; Hou, J.; Tao, X.; Meng, X.; Yang, S. Solution-Processed Electron Transport Layer of n-Doped Fullerene for Efficient and Stable All Carbon Based Perovskite Solar Cells. *J. Mater. Chem. A* **2019**, *7*, 7710–7716.
16. Barichello, J.; Vesce, L.; Matteocci, F.; Lamanna, E.; di Carlo, A. The effect of water in Carbon-Perovskite Solar Cells with optimized alumina spacer. *Sol. Energy Mater. Sol. Cells* **2019**, *197*, 76–83.
17. Alberti, A.; Deretzis, I.; Mannino, G.; Smecca, E.; Giannazzo, F.; Listorti, A.; Colella, S.; Masi, S.; la Magna, A. Nitrogen soaking promotes lattice recovery in polycrystalline hybrid perovskites. *Adv. Energy Mater.* **2019**, *9*, 1803450.
18. Alberti, A.; Bongiorno, C.; Smecca, E.; Deretzis, I.; la Magna, A.; Spinella, C. Pb clustering and PbI_2 nanofragmentation during methylammonium lead iodide perovskite degradation. *Nat. Commun.* **2019**, *10*, 2196.
19. Mannino, G.; Alberti, A.; Deretzis, I.; Smecca, E.; Sanzaro, S.; Numata, Y.; Miyasaka, T.; la Magna, A. First evidence of $CH_3NH_3PbI_3$ optical constants improvement in a N_2 environment in the range 40/80 °C. *J. Phys. Chem. C* **2017**, *121*, 7703.
20. Deretzis, I.; Alberti, A.; Pellegrino, G.; Smecca, E.; Giannazzo, F.; Sakai, N.; Miyasaka, T.; la Magna, A. Atomistic origins of $CH_3NH_3PbI_3$ degradation to PbI_2 in vacuum. *Appl. Phys. Lett*. **2015**, *106*, 131904.
21. Alberti, A.; Smecca, E.; Sanzaro, S.; Mannino, G.; Deretzis, I.; la Magna, A. Hybrid perovskites for photovoltaics: Story, challenges and opportunities. *Riv. Nuovo Cim.* **2019**, *7*, 301–366.
22. Zhang, H.; Xiao, J.; Shi, J.; Su, H.; Luo, Y.; Li, D.; Wu, H.; Cheng, Y.B.; Meng, Q. Self-Adhesive Macroporous Carbon Electrodes for Efficient and Stable Perovskite Solar Cells. *Adv. Funct. Mater.* **2018**, *28*, 1802985.
23. Valastro, S.; Smecca, E.; Sanzaro, S.; Deretzis, I.; la Magna, A.; Numata, Y.; Jena, A.K.; Miyasaka, T.; Gagliano, A.; Alberti, A. Full Efficiency Recovery in Hole-Transporting Layer-Free Perovskite Solar Cells With Free-Standing Dry-Carbon Top-Contacts. *Front. Chem.* **2020**, *8*, doi: 10.3389/fchem.2020.00200.
24. Back, H.; Kim, G.; Kim, H.; Nam, C.Y.; Kim, J.; Kim, Y.R.; Kim, T.; Park, B.; Durrant, J.R.; Lee, K. Highly stable inverted methylammonium lead tri-iodide perovskite solar cells achieved by surface re-crystallization. *Energy Environ. Sci*. **2020**, *13*, 840–847.
25. Khenkin, M.V.; Katz, E.A.; Abate, A.; Bardizza, G.; Berry, J.J.; Brabec, C.; Brunetti, F.; Bulović, V.; Burlingame, Q.; Di Carlo, A.; et al. Consensus statement for stability assessment and reporting for perovskite photovoltaics based on ISOS procedures *Nat. Energy* **2020**, *5*, 35–49.
26. Ceratti, D.R.; Rakita, Y.; Cremonesi, L.; Tenne, R.; Kalchenko, V.; Elbaum, M.; Oron, D.; Potenza, M.A.C.; Hodes, G.; Cahen,D. Self-Healing Inside APbBr3 Halide Perovskite Crystals. *Adv. Mater.* **2018**, *30*, 1706273.
27. Schulz, P.; Cahen, D.; Kahn, A. Halide perovskites: Is it all about the interfaces? *Chem. Rev.* **2019**, *119*, 3349–3417.
28. Shao, S.; Loi, M.A. The Role of the Interfaces in Perovskite Solar Cells. *Adv. Mater. Interfaces* **2020**, *7*, 1901469.